Cement and Concrete Research 38 (2008) 1061–1069

Contents lists available at ScienceDirect

Cement and Concrete Research

journal homepage: http://ees.elsevier.com/CEMCON/default.asp

Effect of specimen size on fracture energy and softening curve of concrete: Part II. Inverse analysis and softening curve

Seung Hee Kwon [a], Zhifang Zhao [b], Surendra P. Shah [c,*]

[a] Assistant Professor, Department of Civil and Environmental Engineering, Myongji University, San 38-2 Namdong, Cheoingu, Yongin, Gyeonggi-do, 449-728, Republic of Korea
[b] Professor of College of Civil Engineering and Architecture, Zhejiang University of Technology, Hangzhou, Zhejiang 310014, PR China
[c] Northwestern University, 2145 Sheridan Road, A130, Evanston, IL. 60208, USA

ARTICLE INFO

Article history:
Received 22 October 2007
Accepted 18 March 2008

Keywords:
Softening curve
Inverse analysis
Size effect
Fracture process zone

ABSTRACT

The size effect of fracture energy was observed in experiments presented in the preceding paper. In this paper, the softening curve representing the relationship between the crack opening and the gradual stress drop after tensile strength was found for each specimen of the experiments by an inverse analysis. The effect of the size-dependent fracture energy on the softening curve was then investigated. It was found that the first steep branch of the softening curve is very similar for different size specimens whereas the tail of the curve becomes longer with increased specimen size. The observed size-dependent fracture energy can be explained by the features identified on the softening curve, and a possible mechanism of the fracture process zone with respect to the size effect is discussed herein.

© 2008 Elsevier Ltd. All rights reserved.

1. Introduction

A softening curve is representing the relationship between the crack opening displacement and the gradual stress drop after the tensile strength. It is commonly used in the simulation of tensile cracking of concrete. The crack band model [1] and cohesive crack model [2] are representative approaches in practical finite element analyses for cracking. In the former, the softening behavior is incorporated with the elastic behavior in an element by scaling the softening curve according to the element size. In the latter, the crack path coincides with boundaries between elements, and the softening curve directly represents the relationship between transverse displacement of the boundaries and the corresponding cohesive force. One advantage of the softening curve is that it fully describes the fracture process zone (FPZ). However, the fracture process zone is simplified: it is lumped into a line in the cohesive crack model, and its inelastic deformation is smeared over a band of elements exhibiting softening behavior in the crack band model. The lattice model [3,4] and nonlocal damage model [5] are among some of the approaches that enable a more realistic simulation of the FPZ, including its width and length. Although these methods are useful for understanding the fracture process and determining the interactions between the characteristics in different scales, there are limitations in computational effectiveness, three-dimensional modeling, and predictive capability.

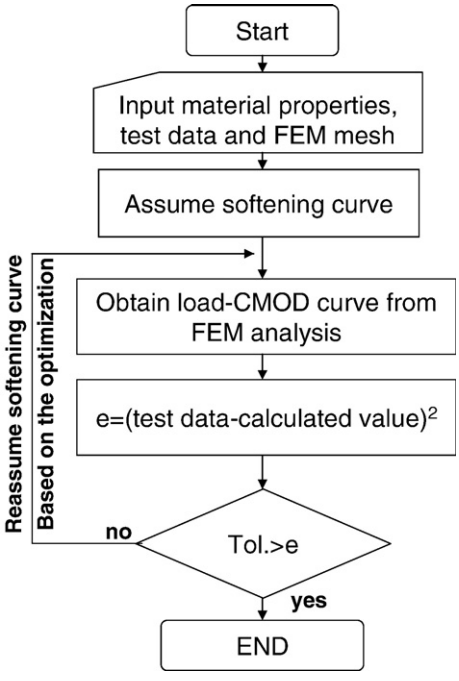

Fig. 1. Algorithm of inverse analysis.

* Corresponding author.

0008-8846/$ – see front matter © 2008 Elsevier Ltd. All rights reserved.
doi:10.1016/j.cemconres.2008.03.014

In this study, softening curves for every specimen assessed in the companion paper were found by inverse analyses, in which the cohesive crack model was employed and the softening curve was assumed to be a tetra-linear curve. From the analysis results, we identified how the size effect of fracture energy observed in the preceding paper [6] affects the softening curve and also examined the differences in the softening curves of the beam and wedge splitting specimens to assess if there is indeed a geometry effect. Finally, a possible mechanism for the FPZ with respect to the size effect has been discussed.

2. Inverse analysis and softening curve

2.1. General

In order to find the softening curve that optimally fits the measured load–CMOD curve, a finite element analysis and an optimization technique were incorporated. The algorithm of the inverse analysis is shown in Fig. 1. Fig. 2 shows the finite element meshes for the beam and wedge splitting specimens; the meshes were scaled up or down according to the specimen size. Only half of

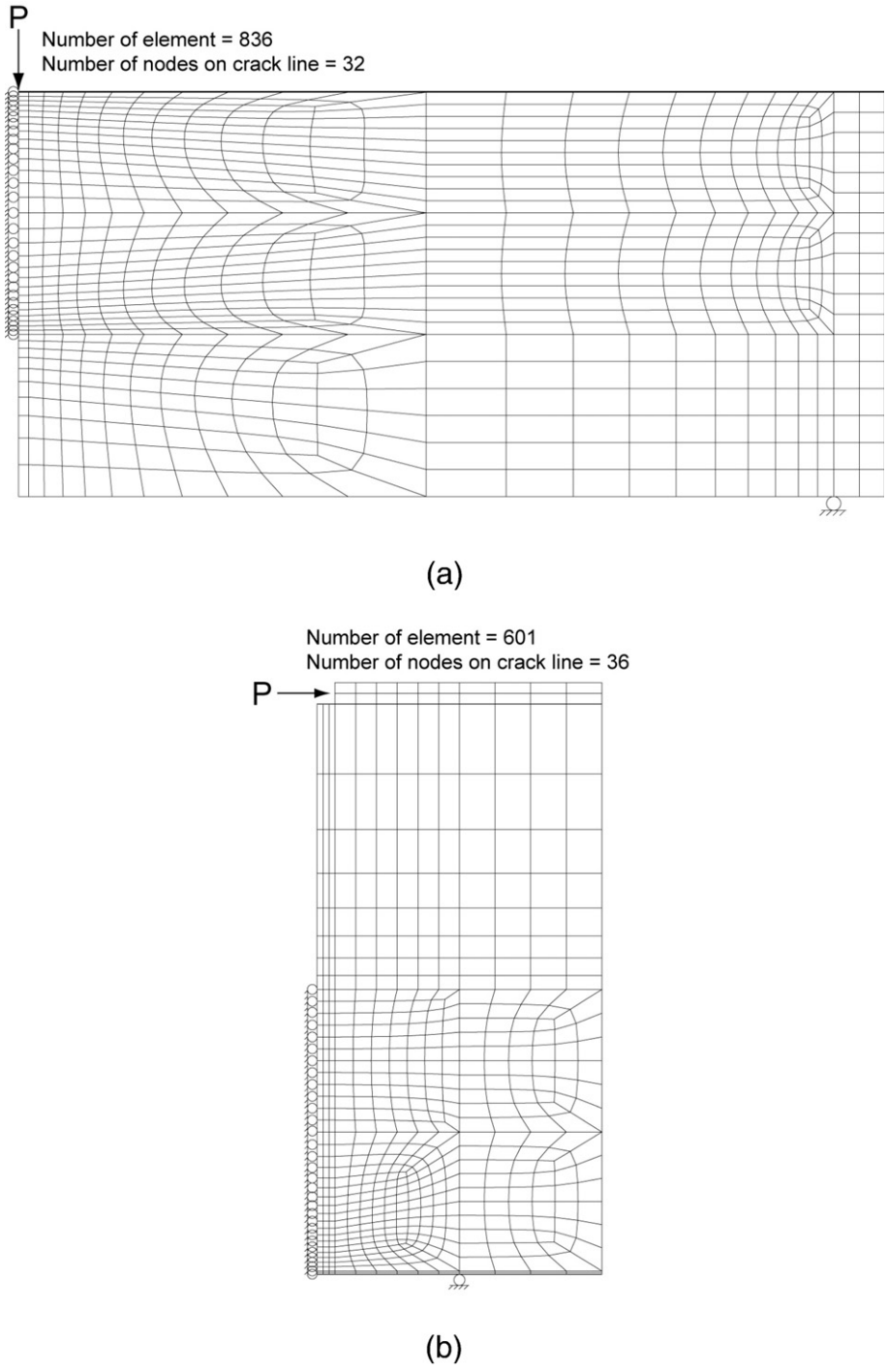

Fig. 2. Specimen configuration and finite element mesh. (a) Beam specimen. (b) Wedge splitting specimen.

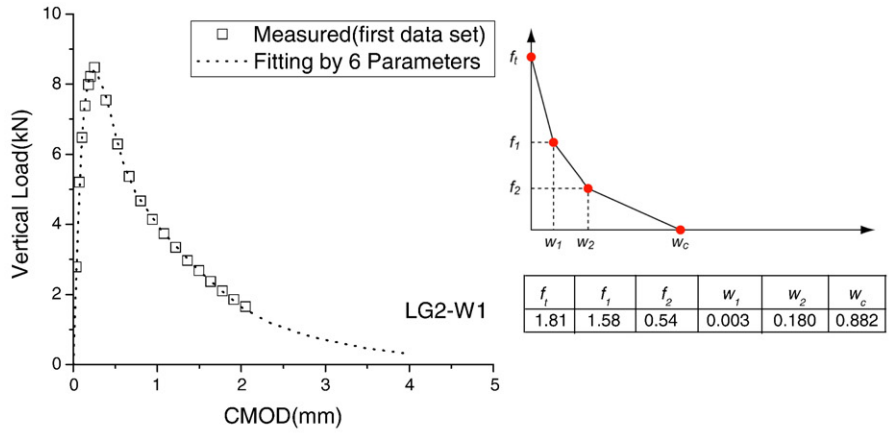

(a)

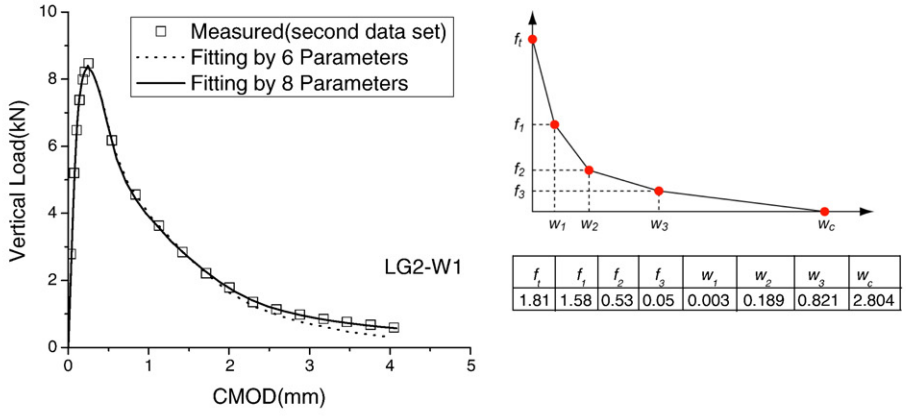

(b)

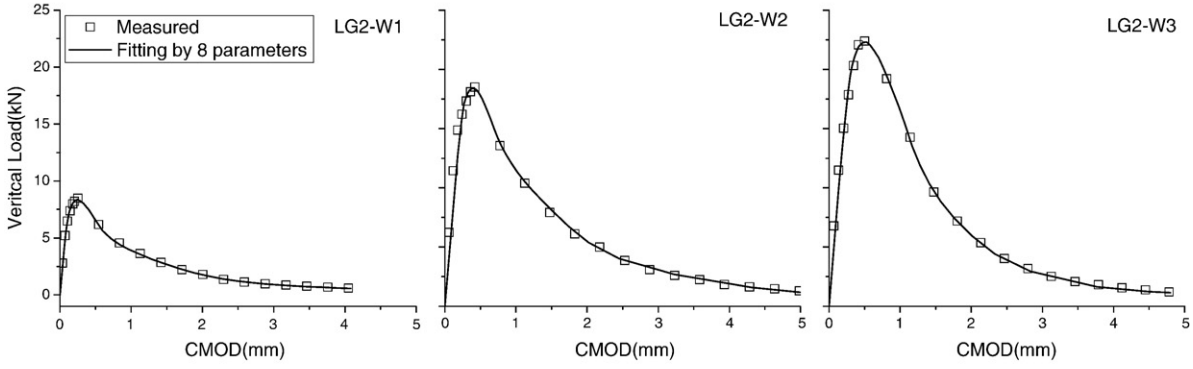

(c)

Fig. 3. Procedure of inverse analysis. (a) First curve fit using 6 parameters. (b) Second curve fit using 8 parameters. (c) Curve fit results for LG2 series.

the specimen was modeled, considering its symmetry. The total number of elements and the number of nodes on the ligaments were 836 and 32 for the beam specimen and 601 and 36 for the wedge splitting specimen, respectively. The cohesive crack model and the principle of superposition suggested by Gopalaratnam and Ye [7] were employed to simulate the crack propagation. The stress condition was assumed as plane stress, and the initial tangent modulus, listed in the preceding paper [6], was used as a material input for the elastic body. The overall optimization procedure was the same as that employed in a previous study [8] with the exception that the Marquardt–Levenberg method [9] was used instead of the Newton–Raphson iteration method.

Table 1
Parameters of tetra-linear softening curve for each specimen

Specimens			8 parameters of softening curve							
			f_t (MPa)	f_1 (MPa)	f_2 (MPa)	f_3 (MPa)	w_1 (mm)	w_2 (mm)	w_3 (mm)	w_c (mm)
Beam	SG1	B1	1.95	1.01	0.43	0.17	0.074	0.183	0.359	0.728
		B2	3.30	1.46	0.59	0.22	0.032	0.113	0.350	1.224
		Avr.	2.63	1.44	0.64	0.19	0.034	0.116	0.332	1.224
	SG2	B1	3.74	1.32	0.51	0.10	0.041	0.131	0.280	0.571
		B2	3.36	1.38	0.83	0.28	0.046	0.072	0.196	0.566
		B3	3.91	1.98	0.60	0.23	0.017	0.105	0.230	0.724
		B4	4.14	1.30	0.65	0.35	0.036	0.108	0.224	0.828
		B5	3.68	3.15	0.66	0.21	0.013	0.063	0.222	0.604
		Avr.	3.78	1.68	0.77	0.23	0.033	0.076	0.220	0.828
	SG3	B1	4.45	2.63	0.57	0.18	0.012	0.085	0.226	0.490
	SG4	B1	4.85	1.48	0.67	0.19	0.027	0.105	0.206	0.726
	SG5	B1	3.59	1.20	0.54	0.20	0.052	0.099	0.210	0.384
	SG6	B1	1.96	1.86	0.89	0.30	0.034	0.074	0.204	0.656
	LG1	B1	2.76	1.63	0.59	0.25	0.003	0.151	0.502	1.151
		B2	2.62	1.80	0.59	0.25	0.009	0.144	0.451	0.854
		B3	3.76	1.75	0.58	0.19	0.010	0.171	0.603	1.084
		B4	3.48	1.42	0.67	0.34	0.023	0.154	0.316	0.990
		Avr.	3.16	2.05	1.51	0.42	0.007	0.024	0.188	1.151
	WG1	B1	4.32	2.22	0.63	0.14	0.010	0.055	0.261	0.642
		B2	3.95	1.61	0.53	0.24	0.022	0.121	0.344	0.810
		B3	3.21	1.52	0.46	0.26	0.019	0.149	0.322	1.068
		Avr.	3.83	1.80	0.89	0.26	0.017	0.062	0.196	1.068
Wedge	SG1	W1	3.39	1.58	0.42	0.10	0.004	0.132	0.350	0.702
		W2	3.61	1.72	0.45	0.12	0.005	0.147	0.503	1.102
		Avr.	3.50	1.68	0.44	0.09	0.004	0.139	0.438	1.102
	SG2	W1	3.36	1.85	0.43	0.18	0.024	0.135	0.281	0.860
		W2	4.11	1.69	0.45	0.05	0.032	0.238	0.580	1.371
		W3	3.30	1.40	0.26	0.12	0.062	0.338	0.705	1.471
		W4	3.29	1.36	0.71	0.33	0.069	0.243	0.378	1.103
		Avr.	3.52	2.03	1.08	0.11	0.031	0.086	0.387	1.471
	SG3	W1	3.93	1.52	0.14	0.04	0.044	0.208	0.702	1.006
	SG4	W1	3.24	1.84	0.21	0.08	0.008	0.148	0.352	0.673
	SG5	W1	4.78	2.19	0.63	0.10	0.021	0.137	0.241	0.596
	SG6	W1	3.75	2.40	0.97	0.20	0.006	0.102	0.372	0.904
	LG2	W1	1.81	1.58	0.53	0.05	0.003	0.189	0.821	2.804
		W2	3.77	1.78	0.71	0.12	0.022	0.241	0.818	2.050
		W3	2.27	1.52	0.38	0.01	0.095	0.410	0.991	2.453
		Avr.	2.62	1.72	0.69	0.08	0.023	0.235	0.766	2.804
	WG2	W1	3.47	1.51	0.37	0.10	0.015	0.152	0.328	0.502
		W2	4.47	1.50	0.31	0.04	0.025	0.267	0.703	1.662
		W3	4.89	1.50	0.35	0.13	0.029	0.364	0.708	1.472
		Avr.	4.28	1.57	0.69	0.12	0.024	0.159	0.400	1.662

2.2. Procedure of inverse analysis

Fig. 3 shows the procedure of the inverse analysis to find the tetra-linear softening curve optimally fitting the measured load–CMOD curve for each specimen. Two test data sets were prepared prior to the inverse analysis; the data extraction method was described in the preceding paper [6]. The first set consists of 20 points (8 points in the ascending part, 12 points in the descending part), and the last CMOD of the first set is almost half of the largest CMOD measured in the test. In the second set, which also consists of 20 points, the ascending part is the same as in the first set, and the descending part is roughly twice longer than that of the first set.

In the first step of the inverse analysis, the tri-linear softening curve optimally fitting the first data set was found, as shown in Fig. 3 (a), and six parameters of the tri-linear curve were obtained. In the second step, three parameters obtained from the first curve fit, f_t, f_1, and w_1, which do not affect the tail part of the load–CMOD curve, were fixed and the remaining five parameters among the eight parameters of the tetra-linear curve fitting the second data set were found, as shown in Fig. 3(b). As shown in the left graph of Fig. 3(b), the tetra-linear softening curve can more accurately fit the tail part of the load–CMOD curve. Fig. 3(c) shows the test data and the curve fit results for the LG2 series. Because of the different sensitivities of each parameter, it is difficult to directly find tetra-linear curve. In a number of studies [7,8,10], a bi-linear softening curve has been employed to simulate tensile cracking of concrete, owing to its simplicity. However, comparing the results from a previous study using a bi-linear softening curve in the optimization [8], it is found that the tetra-linear curve can much more accurately fit the measured load–CMOD curve, as shown in Fig. 3(c).

2.3. Softening curves from the inverse analysis and averaging softening curves

Table 1 shows the eight parameters of the tetra-linear softening curve for every specimen. The eight parameters of the softening curves for different size specimens were averaged and are shown in Table 1. Fig. 4 schematically illustrates how the averaged softening curve was obtained. For example, when two softening curves are averaged, the stress is averaged at 10 points of two tetra-linear softening curves, as shown in Fig. 4(a). Because the first point is the tensile strength f_t, a total of nine averaged points can be obtained. The

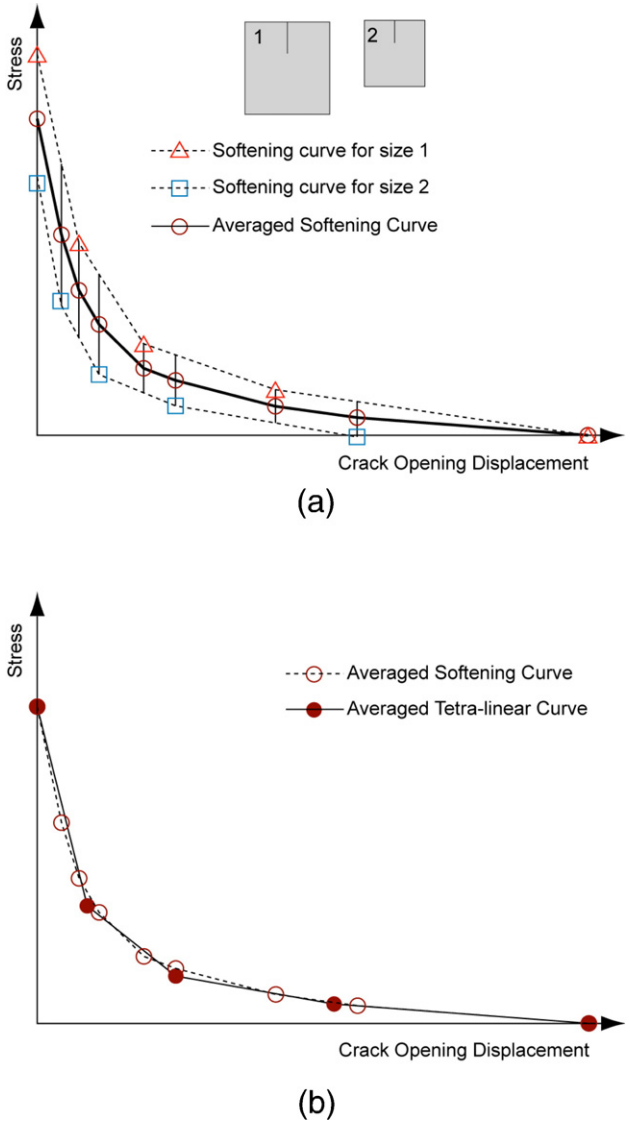

Fig. 4. Averaging method for softening curves of different size specimens. (a) Averaging softening curves for different size specimens. (b) Averaged tetra-linear softening curve.

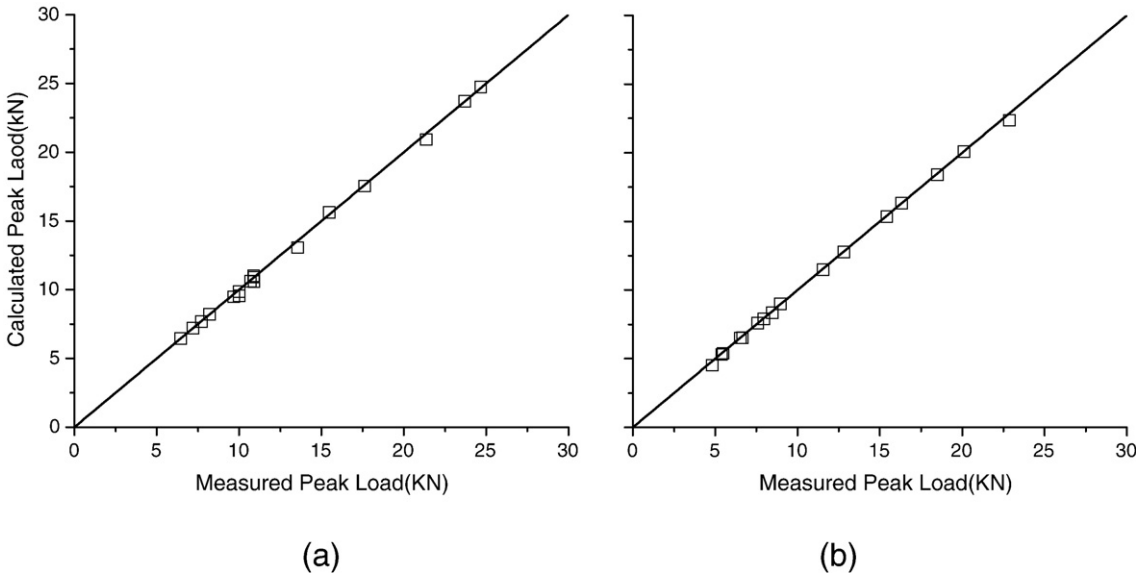

Fig. 5. Comparison between measured and calculated peak load (based on the optimized softening curve). (a) Beam test. (b) Wedge splitting test.

averaged curve now consists of 9 points. This was then converted to tetra-linear curve by optimization process, as shown in Fig. 4(b).

3. Analysis results and discussion

3.1. Comparison between the measured and calculated peak load and CMOD at peak

The peak loads obtained from the optimized softening curves of Table 1 for all the specimens are compared to the measured peak loads in Fig. 5, and excellent agreement between the measured and calculated results in both the beam and wedge splitting tests can be seen. The calculated and measured CMOD at peak are compared in Fig. 6, and every point is also very closely distributed to the 45° linear line. A comparison between the fracture energy calculated based on the optimized softening curve, which means the area under the softening curve, and the experimentally measured fracture energy is presented in Fig. 7. While the calculated and measured fracture energy are very close to each other in the wedge splitting test in Fig. 7 (b), the calculated values are slightly lower than the measured results in the beam test. In the case of the beam test, the measured fracture energy was obtained from the load–deflection curve and the optimized softening curve was found by fitting the load–CMOD curve. The differences among the fracture energies of Fig. 7(a) indicate that a part of the externally applied energy to the beam specimen was dissipated due to spurious energy loss, rather than due to the crack formation. The possible sources were noted in the preceding paper [6]. From Figs. 3(c) and 5–7, it can be confirmed that the softening curves found from the inverse analysis accurately simulate the fracture response.

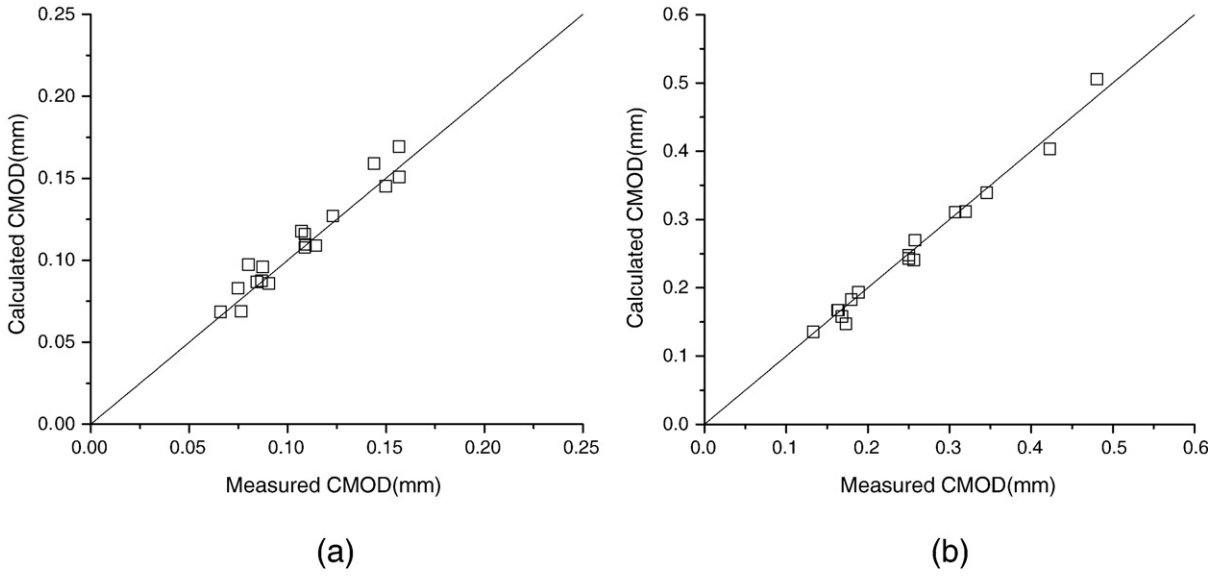

Fig. 6. Comparison between measured and calculated CMOD at peak (based on the optimized softening curve). (a) Beam test. (b) Wedge splitting test.

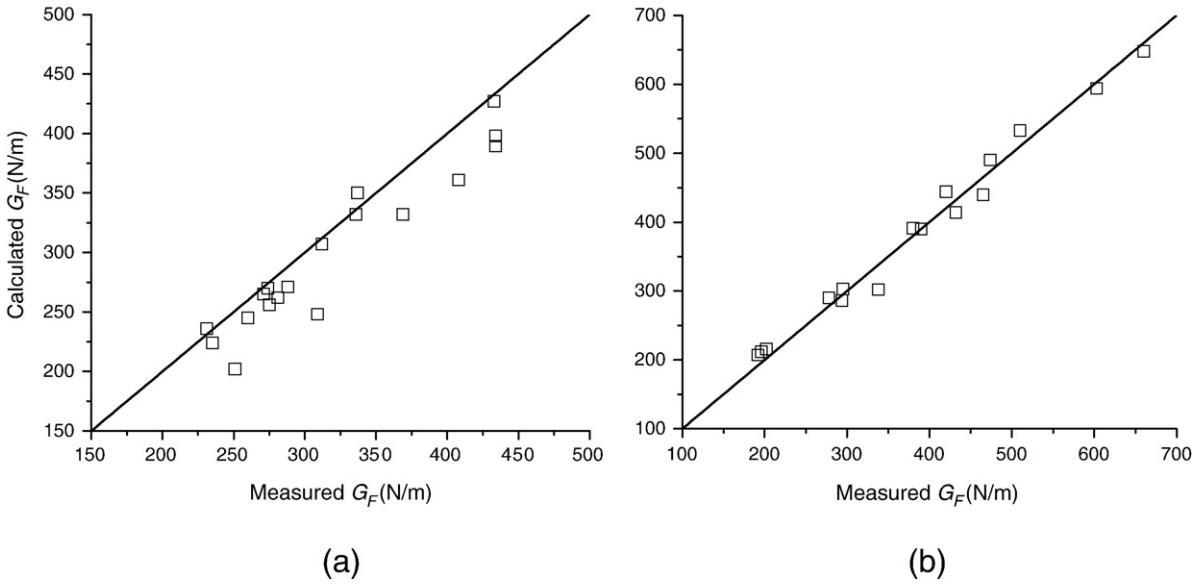

Fig. 7. Comparison between measured and calculated G_F (based on the optimized softening curve). (a) Beam test. (b) Wedge splitting test.

Peak load and corresponding CMOD for specimens of different size were calculated from the averaged softening curve and are compared to the measured values in Figs. 8 and 9. Although the scatter is larger than that of Figs. 5 and 6, good agreement between the measured and calculated values is still obtained. From the initial loading to the peak load state, the fracture process zone is not fully developed and the cohesive stress at the initial crack tip or the end point of the initial notch remains in the first steep branch of the softening curve. Even for a specimen of infinite size, the cohesive stress at the initial crack tip is almost at the end of the first branch [11]. Therefore, the accurate fit of the averaged softening curve to the peak load and corresponding CMOD indicates that the initial steep branch of the softening curve does not depend on the specimen size; or, even if it depends on the size, the effect of the size on the initial branch is small enough to ignore. If the initial branch is similar for the different size specimens, then the remaining part of the softening curve should depend on the size to equilibrate the experimentally observed size-dependent fracture energy.

Based on the averaged curve for specimens of different size, the softening curve of each specimen was re-determined. The four stress parameters of the averaged softening curve, f_t, f_1, f_2, and f_3, were fixed and the four COD parameters, w_1, w_2, w_3, w_c, optimally fitting the first found softening curve for each specimen were then found, as listed in Table 2.

The softening curves of the beam and wedge splitting specimens for SG3 to SG6 were also averaged using the method described in Fig. 4, and the results are listed in Table 3. The four COD parameters for the beam and wedge specimens, w_1, w_2, w_3, w_c, were re-determined, fixing the parameters f_t, f_1, f_2, and f_3 as given in Table 2. The results are shown in Table 3.

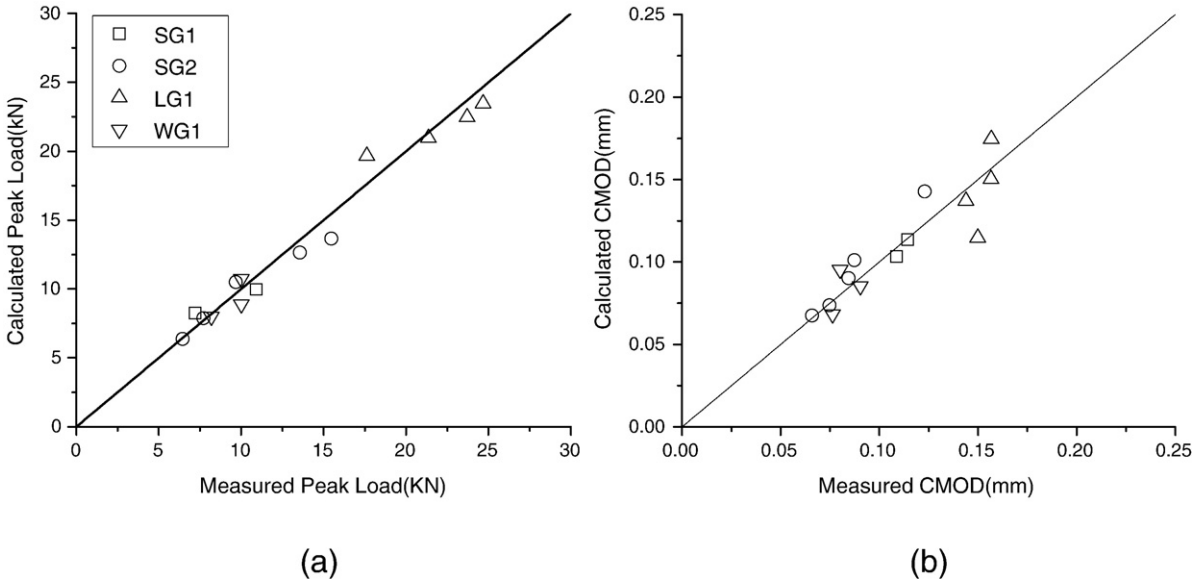

Fig. 8. Comparison between measured and calculated peak load and CMOD at peak for beam specimens (based on the averaged softening curve). (a) Peak load. (b) CMOD at peak.

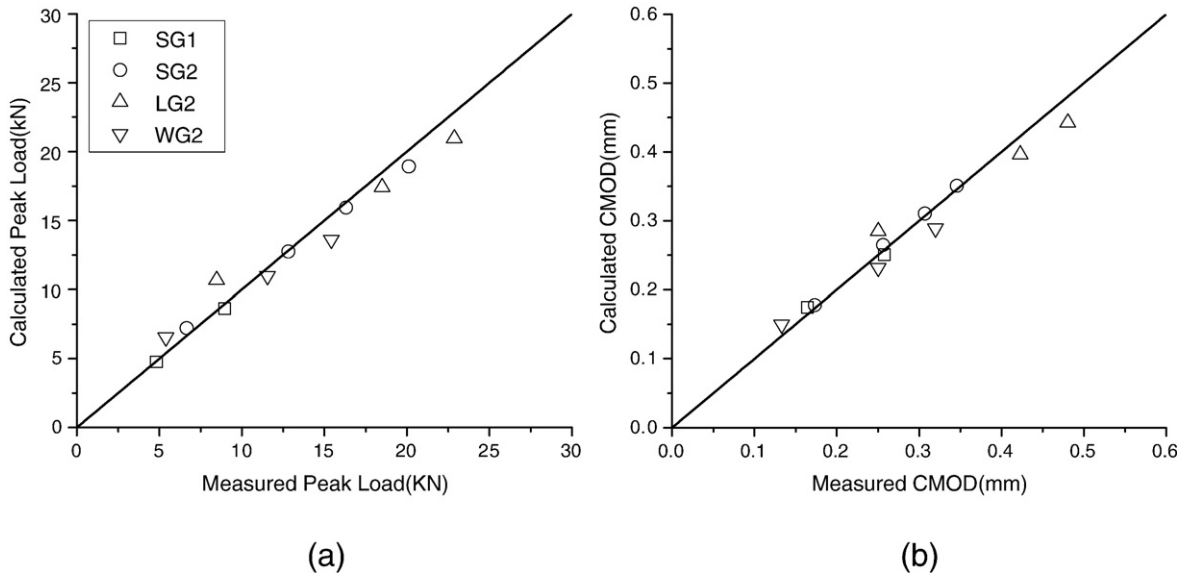

Fig. 9. Comparison between measured and calculated peak load and CMOD at peak for wedge splitting specimens (based on the averaged softening curve). (a) Peak load. (b) CMOD at peak.

3.2. Effect of ligament length on softening curve

In order to examine the effect of the specimen size on the tailing part softening curve, relative variation of crack opening parameters to the averaged softening curve was analyzed. The relative variation of the crack opening parameters is expressed by the following equation.

$$r_i = s_i v_i = \frac{w_{\mathrm{ia,SG1}} + w_{\mathrm{ia,SG2}} + w_{\mathrm{ia,LG}} + w_{\mathrm{ia,WG}}}{w_{\mathrm{ca,SG1}} + w_{\mathrm{ca,SG2}} + w_{\mathrm{ca,LG}} + w_{\mathrm{ca,WG}}} v_i,\ v_i = \frac{w_i}{w_{ia}} \quad (1)$$

In the equation, r_i is the relative variation of the crack opening parameter, s_i is a scale factor for the whole test series and represents the relative magnitude of the ith COD parameter to the COD at zero cohesive stress, and v_i is the variation ratio of the ith COD parameter (w_i) to the ith COD parameter of the averaged softening curve (w_{ia}). The COD parameter w_i for each specimen is listed in Table 2, and w_{ia} is the COD parameter of the averaged softening curve for the different size specimens, which are listed in Table 1. The relative variation of the crack opening parameter r_i for the beam and wedge splitting specimens of different size is plotted over their ligament length, as shown in Fig. 10. In Fig. 10, the 45° line is the regression line for each r_i. In both the beam and wedge splitting specimens, r_c corresponding to w_c increases with an increase of the ligament length, and the effect of the specimen size or the ligament length on the COD parameter is reduced for the relatively smaller COD parameter. From Figs. 8–10, it can be seen that the initial branch of the softening curve is not greatly affected by the size, and the tail part of the curve becomes longer with an increase of size.

Table 2
Softening curve when stresses are fixed as averaged values

Specimens			8 parameters of softening curve							
			f_t (MPa)	f_1 (MPa)	f_2 (MPa)	f_3 (MPa)	w_1 (mm)	w_2 (mm)	w_3 (mm)	w_c (mm)
Beam	SG1	B1	2.63	1.44	0.64	0.19	0.022	0.135	0.307	0.734
		B2	2.63	1.44	0.64	0.19	0.042	0.104	0.359	1.287
	SG2	B1	3.78	1.68	0.77	0.23	0.034	0.086	0.214	0.431
		B2	3.78	1.68	0.77	0.23	0.034	0.074	0.217	0.591
		B3	3.78	1.68	0.77	0.23	0.021	0.099	0.206	0.737
		B4	3.78	1.68	0.77	0.23	0.033	0.077	0.267	0.960
		B5	3.78	1.68	0.77	0.23	0.043	0.061	0.196	0.599
	LG1	B1	3.16	2.05	1.51	0.42	0.001	0.010	0.195	1.120
		B2	3.16	2.05	1.51	0.42	0.004	0.033	0.177	0.877
		B3	3.16	2.05	1.51	0.42	0.010	0.031	0.207	1.049
		B4	3.16	2.05	1.51	0.42	0.018	0.205	0.201	0.980
	WG1	B1	3.83	1.80	0.89	0.26	0.015	0.050	0.162	0.551
		B2	3.83	1.80	0.89	0.26	0.021	0.078	0.221	0.878
		B3	3.83	1.80	0.89	0.26	0.013	0.082	0.222	1.141
Wedge	SG1	W1	3.50	1.68	0.44	0.09	0.004	0.124	0.355	0.719
		W2	3.50	1.68	0.44	0.09	0.005	0.150	0.546	1.171
	SG2	W1	3.52	2.03	1.08	0.11	0.020	0.075	0.203	1.444
		W2	3.52	2.03	1.08	0.11	0.031	0.104	0.384	1.164
		W3	3.52	2.03	1.08	0.11	0.037	0.094	0.425	1.944
		W4	3.52	2.03	1.08	0.11	0.040	0.098	0.482	2.015
	LG2	W1	2.62	1.72	0.69	0.08	0.0001	0.147	0.701	2.318
		W2	2.62	1.72	0.69	0.08	0.047	0.239	0.872	2.347
		W3	2.62	1.72	0.69	0.08	0.051	0.311	0.670	2.413
	WG2	W1	4.28	1.57	0.69	0.12	0.011	0.108	0.243	0.546
		W2	4.28	1.57	0.69	0.12	0.025	0.177	0.380	1.257
		W3	4.28	1.57	0.69	0.12	0.032	0.245	0.553	1.664

3.3. Comparison between softening curves of beam and wedge splitting tests

The test series of SG3 to SG6 in the preceding paper were designed for a comparison between the different geometries of beam and wedge splitting specimens. Their ligament length is slightly different: 150 mm for the beam specimens and 180 mm for the wedge splitting specimens. Although there is a size effect on the softening curve, a 30 mm difference is not expected to substantially affect the softening

Table 3
Averaged softening curves and softening curves when stresses are fixed as averaged values

Concrete		8 parameters of softening curve							
		f_t (MPa)	f_1 (MPa)	f_2 (MPa)	f_3 (MPa)	w_1 (mm)	w_2 (mm)	w_3 (mm)	w_c (mm)
Average	SG3	4.19	2.64	1.00	0.10	0.016	0.070	0.228	1.006
	SG4	4.05	1.80	0.71	0.20	0.020	0.098	0.175	0.726
	SG5	4.20	2.14	0.78	0.11	0.025	0.096	0.234	0.596
	SG6	2.86	2.27	0.84	0.19	0.005	0.099	0.334	0.904
Beam	SG3-B1	4.19	2.64	1.00	0.10	0.013	0.067	0.192	0.797
	SG4-B1	4.05	1.80	0.71	0.20	0.027	0.088	0.209	0.711
	SG5-B1	4.20	2.14	0.78	0.11	0.026	0.071	0.215	0.476
	SG6-B1	2.86	2.27	0.84	0.19	9.5×10^{-9}	0.084	0.240	0.729
Wedge	SG3-W1	4.19	2.64	1.00	0.10	0.020	0.069	0.243	1.034
	SG4-W1	4.05	1.80	0.71	0.20	0.007	0.107	0.144	0.567
	SG5-W1	4.20	2.14	0.78	0.11	0.025	0.124	0.231	0.584
	SG6-W1	2.86	2.27	0.84	0.19	0.018	0.110	0.399	0.904

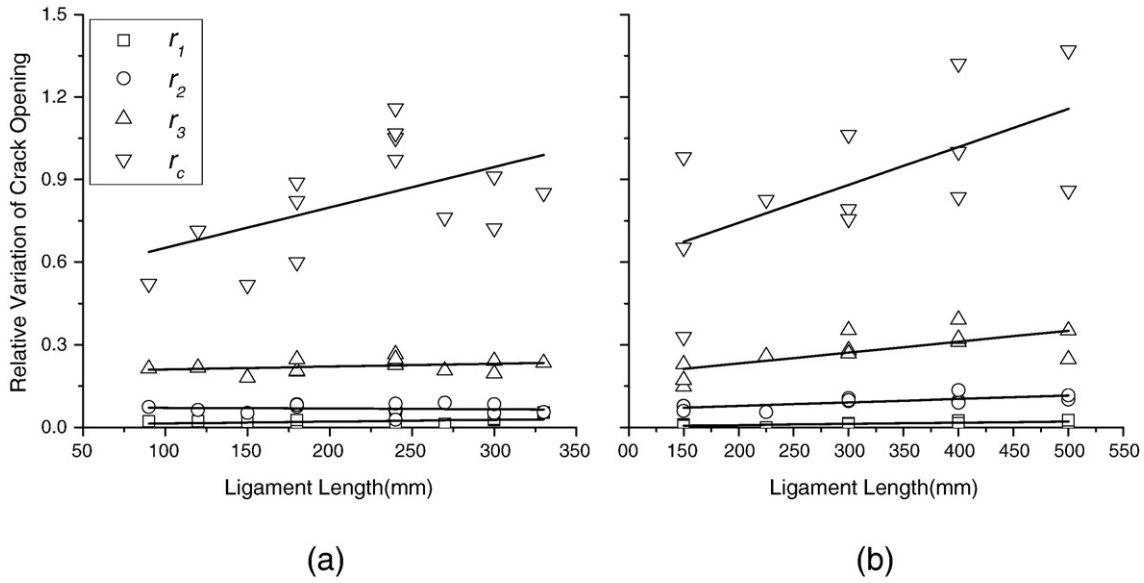

Fig. 10. Relative variation of crack opening according to ligament length. (a) Beam specimens. (b) Wedge splitting specimens.

curve, and would not influence a comparison between softening curves of the beam and wedge splitting specimens. For the comparison, the variation ratio v_i defined above was calculated from Table 3 and is shown in Fig. 11. Variation of the parameters w_1, w_2 and w_3 between the beam and wedge specimens is not large and there is no specific trend according to the different geometry. In contrast with parameters, w_c of the wedge specimen is much larger than that of the beam specimen. Similar to the size effect of the softening curve, the parameter w_c is largely affected by the geometry.

3.4. Possible mechanism for the size and geometry effect of fracture energy

The correlation of the softening curve to the mechanism of FPZ has been previously studied [12] and is schematically described in Fig. 12 (a). Microcracks start to form immediately before the stress reaches the tensile strength. After the tensile strength is reached, the microcracks are localized and extended in the potential line of a macro visible crack. The first steep branch of the softening curve corresponds to localization and extension of the microcracks. According to the features of the softening curve found above, the process until this fracture stage is not substantially affected by the specimen size or geometry. The stress transmitted to the region where microcracks are distributed by the bridging effect remains even after separation of the crack surface. The region corresponds to the tail of the softening curve and is the origin of the observed size-dependent fracture energy.

As shown above, the tail part becomes longer with an increase of specimen size. In other words, the fracture energy dissipated in the region to which the stress is transmitted by the bridging effect is larger for a larger size specimen. The energy is dissipated in the site of microcracking. If the density of the damage due to the microcracks is uniform according to the size, the area that the bridging affects or the width of FPZ should be larger for the larger size specimen, as shown in Fig. 12(b).

According to previous experimental and analytical studies [12–14], the FPZ is not symmetric and its width varies along the visible crack line. In Hu and Wittmann's [15] work and Hu and Duan's [16] work, the variation of the width along the crack line and the shape of FPZ according to the size result in the observed size-dependent fracture energy. This was analyzed by introducing a local fracture energy concept. Their findings are partly supported by the results of this study.

Although the size effect of the fracture energy was found within the range of specimen size tested in the preceding paper, it is clear that the fracture energy does not continue increasing over the size, and asymptotically approaches a certain value. The width of the FPZ becomes narrow as the crack propagates close to the back boundary of the specimen, which is the end point of the ligament [13,16]. The influence of the boundary on the measured fracture energy might be a major cause of the size-dependent fracture energy and distinctly reduces with an increase of the size. However, a more precise analytical study needs to be carried out in order to fully understand the effect of size and geometry on the softening curve found in this study as well as the size effect and asymptotic feature of the fracture energy.

4. Conclusions

The softening curve was assumed as a tetra-linear curve and found from an inverse analysis for every specimen tested in the preceding paper, and the effect of specimen size and geometry on the softening curve was investigated. The first steep branch of the softening curve is similar for specimens of different size but the tail of the curve becomes longer with an increase of the specimen size. The experimentally observed size-dependent fracture energy can be explained by the

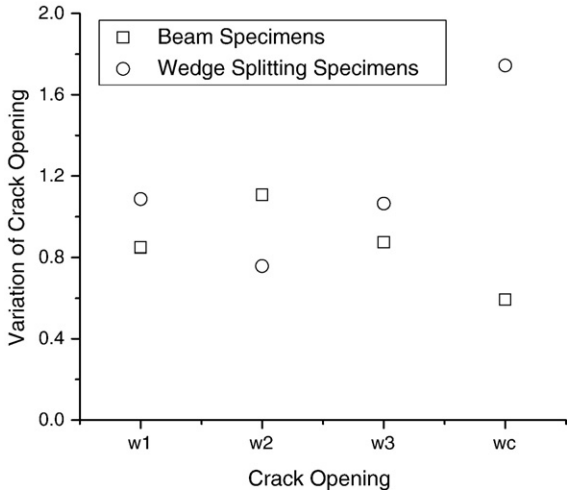

Fig. 11. Variation of crack opening according to specimen type (SG3 to SG6).

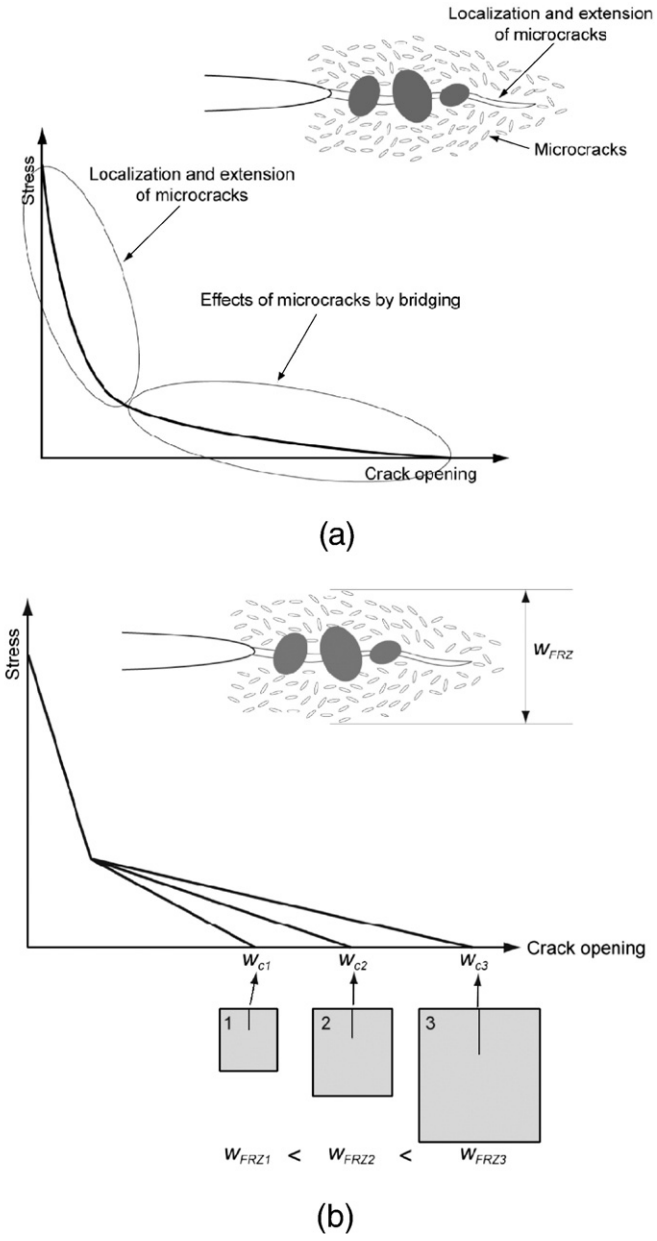

Fig. 12. Possible mechanism on size effect of fracture energy (continue). (a) Correlation of tension softening curve and FPZ. (b) Size-dependent softening curve.

observed features on the softening curve. Finally, a possible mechanism of the fracture process zone with respect to the size effect and asymptotic feature was discussed. In the future, a more precise analytical study needs to be carried out in order to fully understand the effect of size and geometry on the softening curve as well as the size effect and asymptotic feature of the fracture energy.

Notation

CMOD Crack mouth opening displacement
COD Crack opening displacement
f_t, f_1, f_2, f_3 Stress parameters of tetra-linear softening curve
w_1, w_2, w_3, w_c Crack opening parameters of tetra-linear softening curve
r_i Relative variation of crack opening parameter
s_i Scale factor representing the relative magnitude of i^{th} COD parameter to the COD at zero cohesive stress
v_i Variation ratio of the i^{th} COD parameter to the i^{th} COD parameter of the averaged softening curve
w_i i^{th} COD parameter
w_{ia} i^{th} COD parameter of the averaged softening curve

Acknowledgment

This work was partly supported by a Korea Research Foundation Grant (KRF-2005-214-D00063).

References

[1] Z.P. Bazant, B.H. Oh, Crack band theory for fracture of concrete, Materials and Structures 16 (1983) 155–177.
[2] A. Hillerborg, M. Modeer, P.E. Petersson, Analysis of crack formation and crack growth in concrete by means of fracture mechanics and finite elements, Cement and Concrete Research 6 (6) (1976) 773–782.
[3] G. Cusatis, Z.P. Bazant, L. Cedolin, Confinement-shear lattice model for concrete damage in tension and compression: I. theory, ASCE Journal of Engineering Mechanics 129 (12) (2003) 1439–1448.
[4] G. Cusatis, Z.P. Bazant, L. Cedolin, Confinement-shear lattice model for concrete damage in tension and compression: II. computation and validation, ASCE Journal of Engineering Mechanics 129 (12) (2003) 1449–1458.
[5] Z.P. Bazant, G. Pijaudier-Cabot, Nonlocal continuum damage localization instability and convergence, ASME Journal of Applied Mechanics 55 (1988) 287–293.
[6] Z. Zhao, S.H. Kwon, S.P. Shah, Effect of specimens size on fracture energy and softening curve, Cement and Concrete Research (2007) Submitted with the this manuscript.
[7] V.S. Gopalaratnam and B.S. Ye, Numerical characterization of the nonlinear fracture process in concrete, Engineering Fracture Mechanics, 40(6).
[8] J.K. Kim, Y. Lee, S.T. Yi, Fracture characteristics of concrete at early ages, Cement and Concrete Research 34 (2004) 507–519.
[9] K.M. Brown, Derivative-free analogues of the levenberg, Marquardt and Gauss Algorithms for Non-linear Least Square Approximations. IBM, Philadelphia Scientific Center Technical Report, No. 320–2994, 1970.
[10] S.H. Kwon and S.P. Shah, Model to Predict Early-Age Cracking of Fiber-Reinforced Concrete due to Restrained Shrinkage, ACI Material Journal, Submitted for publication.
[11] Z.P. Bazant, J. Planas, Fracture and Size Effect in Concrete and Other Quasibrittle Materials, CRC Press, New York, 1998.
[12] N. Nomura, H. Mihashi, M. Izumi, Correlation of fracture process zone and tension softening behavior in concrete, Cement and Concrete Research 21 (1991) 545–550.
[13] J.P.B. Leite, V. Slowik, H. Mihashi, Computer simulation of fracture processes of concrete using mesolevel models of lattice structures, Cement and Concrete Research 34 (2004) 1025–1033.
[14] L. Cedolin, S.D. Poli, I. Iori, Experimental determination of the fracture process zone in concrete, Cement and Concrete Research 13 (1983) 557–567.
[15] X.Z. Hu, F.H. Wittmann, Fracture energy and fracture process zone, Materials and Structures 25 (1992) 319–326.
[16] X.Z. Hu, K. Duan, Influence of fracture process zone height on fracture energy of concrete, Cement and Concrete Research 34 (2004) 1321–1330.